2014 IEEE International Conference on Robotics & Automation (ICRA)
Hong Kong Convention and Exhibition Center
May 31 - June 7, 2014. Hong Kong, China

A study of the passive rebound behavior of bipedal robots with stiff and different types of elastic actuation

Katayon Radkhah and Oskar von Stryk

***Abstract*— One of the most important capabilities of bipedal robots for energy-efficient and dynamic locomotion are shock tolerance and energy storage and release. In this paper, we study three robot models with different leg actuation designs by means of highly detailed multibody system dynamics simulation. For this purpose, we first elaborate on the term of energy-efficient and dynamic two-legged hopping and present a performance index. Subsequently we conduct the same experimental setup for passive rebound and soft landing for all models. Among others it is observed that (1) the envisioned dynamic and energy-efficient locomotion cannot be achieved through stiff actuation, (2) the energy restitution can be maximized without sacrificing the dynamic mobility and (3) such passive rebound experiments are well suited to determining the optimal leg actuation design.**

I. Introduction

Elastically actuated legs containing mechanical elasticities have some preeminent advantages: (1) shock tolerance, i.e. impacts are absorbed by the springs before they can reach the motors and cause any damage to them, and (2) energy storage and release, which we refer to as *energy restitution*. These advantages were perceived more and more with the advent of the series elastic actuator (SEA) [1] that was originally developed solely for a more accurate and stable force/torque control. Many authors have recognized the previously named benefits as essential properties of a bipedal system for running or jumping motions [2]–[7].

The goal of this paper is to study the requirements for good passive rebound and soft landing in simulation, evaluate these capabilities and use the insights gained for an overall optimal locomotion behavior of the robot. The study is inspired by early passive rebound experiments on the BioBiped1 robot with the purpose of globally validating the overall robot design [8]. The BioBiped1 robot built within the BioBiped project [9] is a biomechanically inspired musculoskeletal humanoid robot comprising active and passive mono- and biarticular muscle-tendon structures. The long-term goal is to achieve three-dimensional (3D) hopping, running and walking (in this order), including performing transitions between these gaits, and standing within a single kinematic leg design.

The focus of the passive rebound experiments was placed on investigating the repulsive leg function, which is directed mainly towards the capability to generate sufficient repulsive leg forces during stance phase to achieve clear flight phases. As shown in Fig. 1, the robot was dropped in a slightly flexed leg configuration from a height of 15 cm. The motors of the knee and ankle joint extension tendons were PD controlled to constantly keep their initial joint position. The ground reaction forces (GRF), displayed in Fig. 2, were measured by a padded Kistler measurement force plate. It could be observed that the robot was able to rebound and lift off its weight by about 5 cm. It was capable of rebounding at least twice (cf. Fig. 2). The initiated flight phase between the first and second bounce lasted for about 150 ms (cf. Fig. 2). Thus it can be concluded that the robot is capable of achieving a large energy restitution passively. Further, the mechanical elasticities prevent the transmission of the peaks to the gearboxes. Further, the peaks arriving at the joints and thus motors decrease distally, being smallest at the hip level.

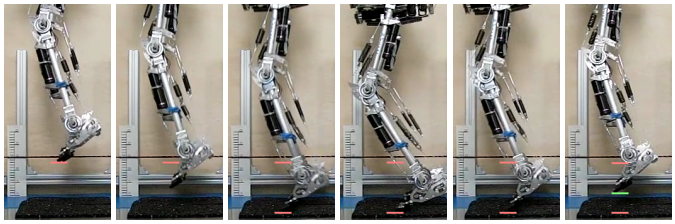

Fig. 1. Passive rebound and soft landing of BioBiped1 after 15 cm drop (timestamps correspond to Fig. 2) [8].

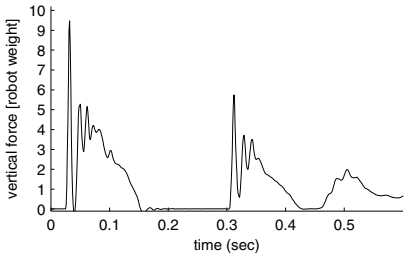

Fig. 2. Vertical ground reaction forces (GRF) of both legs in total during the passive rebound shown in Fig. 1. The forces were measured by a padded Kistler measurement force plate and normalized to BioBiped1's body weight [8].

Musculoskeletal leg designs such as that of BioBiped1 are not yet common and thus the benefits of such systems over conventionally built systems with stiff joints and linear elastic joint actuation may not be completely clarified due to missing experimental and simulation setups allowing such studies. In previous work we derived detailed models of the deployed actuator types [10], created the full multibody system (MBS) dynamics model including the elastic contact mechanics [11] and identified the real robot parameters.

The authors are with the Simulation, Optimization and Robotics Group, Department of Computer Science, Technische Universität Darmstadt, Germany [radkhah,stryk]@sim.tu-darmstadt.de

By means of modeling and simulation at a high level of detail, various different leg actuation designs from stiff to highly compliant actuation involving BioBiped1's complex musculoskeletal system are compared in a specific simulation setup. The goal is to reveal by thorough investigation of the design versus the locomotion performance leg actuation designs suited for dynamic and energy-efficient locomotion. The simulation models with PD controlled joint trajectories are set to a specific configuration and dropped from different heights. The maximum torques arriving at the gearbox together with further selected dynamic performance criteria, such as the passive rebound height and the flight phase initiated by the first bounce, are analyzed and compared among the different leg actuation designs. With this study we confirm not only the well perceived advantage of mechanical compliance in terms of impact absorption but also clarify that the amount of energy storage and release can be maximized without trading off the dynamic mobility. The study is concluded with a summary and discussion of insights gained from the different test cases.

II. Simulation Setup

In order to analyze the passive rebound capabilities various studies are carried out for both stiff and elastic robot models with rotational series elastic joint actuation and active and passive elastic tendon actuation. The models are all dropped from different heights starting at 5 cm and include all a degree of freedom along the pitch axis in the hip, knee and ankle joint. The initial joint angles for the knee and ankle are the same as in the experiment ($q_{\mathrm{Kne}} = -25°$, $q_{\mathrm{Ank}} = -14°$). Additionally, we choose also a slightly flexed configuration for the hip joint with $q_{\mathrm{Hip}} = 10°$. This leg configuration corresponds approximately to that taken at touch-down during synchronous hopping motions. At touch-down the leg is whether fully extended nor flexed. Full extension occurs only at take-off, while full flexion of the legs can be detected at mid-stance. To keep the desired joint positions for the elastic robot models, the corresponding motor positions compensating for the gravitational forces in this leg configuration were determined beforehand based on the actuator models' equations [10].

For the motor-gear units, as deployed in the BioBiped1 robot (RE30 Maxon motors, 60 W, 24 V, with planetary reduction gearbox GP 32C with gear ratio of 66:1), the maximum torques at the gear may not exceed 6 Nm according to the conservative manufacturer's specification. It is assumed that on short term the peak torques arriving at the gearbox may be up to at least twice as high as the specification, i.e. 12 Nm.

The movements of the robot models are completely constrained to 1D. The ground contact model parameters are identical in all studies and given in Table I.

Assuming that the weakest components of the robot system are the motor-gearboxes, and not the segments, which can break as well depending on the impact forces, we wonder:

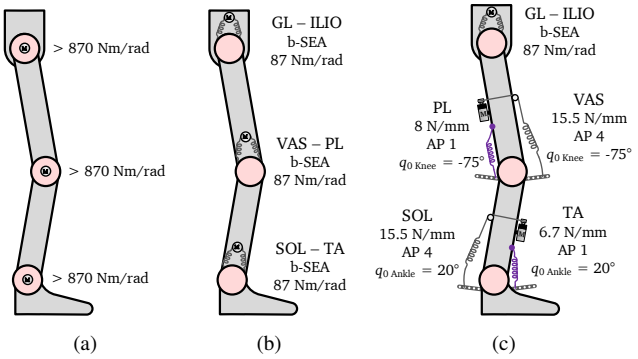

Fig. 3. Simulation models: (a) BioBiped1 robot with completely stiff joint actuation (*stiff robot*), (b) BioBiped1 robot with bidirectional series elastic joint actuation (*b-SEA robot*), (c) validated model of the BioBiped1 robot platform with the given actuation settings (*BioBiped1*).

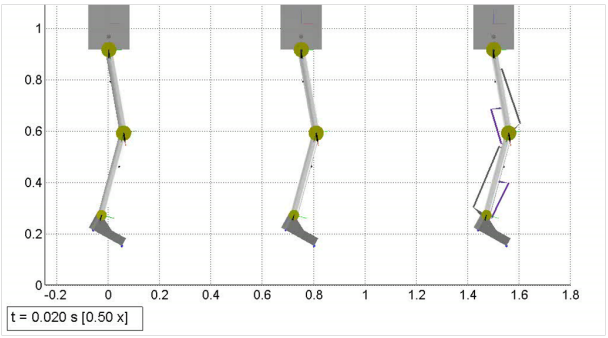

Fig. 4. Snapshot of the simulation as shown in the attached video: on the left the stiff robot, in the middle the b-SEA robot and on the right the validated BioBiped1 robot model.

- Which falling heights cause the maximum peak torques at the gearbox to be exceeded?
- How do the peak torque, GRF, flight phase and energy restitution ratio change for robot systems with different actuator types?
- How does an elastic robot with rotational joint stiffness relate to a stiff robot?
- What is the maximum energy restitution ratio that can be obtained with which actuator type and when is the shock absorption the largest? Is there a trade-off between these two criteria?

A. Models

Three different basis simulation models providing internal variation possibilities are used:

1) *stiff robot*: BioBiped1 robot model with completely stiff joints actuated by geared DC motors (cf. Fig. 3(a)),
2) *b-SEA robot*: BioBiped1 robot model with rotational series elastic joint actuation, i.e. bidirectional SEA (b-SEA) in each joint (cf. Fig. 3(b)),
3) *BioBiped1*: BioBiped1 robot model with active and passive elastic tendon actuation as in the real robot platform (cf. Fig. 3(c)).

For the detailed actuator models' equations we refer to [10]. The segment kinematics and dynamics are identical in all

robot models in terms of link mass and length, center of mass (CoM) and inertia of links. In the stiff robot model the inertia of the links additionally include the reflected rotor and gearbox inertia.

B. Evaluated Performance Measures

The evaluated criteria include the *energy restitution ratio* which is computed from one cycle to another cycle based on the maximum potential energy in each flight phase considering the potential energy when the robot is at rest. To compute the potential energy of the robot's CoM due to the vertical velocity we use $E_{\mathrm{pot}} = m\,g\,h$ with m and g denoting the total mass of the robot and the gravitational acceleration constant, respectively, and $h = z_{\mathrm{CoM}}$.

Further included, to assess the degree of *dynamic mobility*, are the achieved *hopping height* and *ground clearance* after each support phase, the *duty factor*, which refers to the duration of the stance phase relative to the flight phase, and the measured *flight phase*. The hopping height is determined by measuring the vertical fluctuations of the robot's CoM within a cycle. The CoM course during a cycle, $\boldsymbol{p}_{\mathrm{CoM}}$, can be derived either by the GRF or updated by the according link CoM, $\boldsymbol{p}_{\mathrm{CoM\,i}}$, via the following formula:

$$\boldsymbol{p}_{\mathrm{CoM}} = \begin{pmatrix} x_{\mathrm{CoM}} \\ y_{\mathrm{CoM}} \\ z_{\mathrm{CoM}} \end{pmatrix} = \frac{\sum m_i\,\boldsymbol{p}_{\mathrm{CoM\,i}}}{\sum m_i}\,. \tag{1}$$

Subsequently, the hopping height can be computed as the deviation of the apex, the maximum CoM position along the z-axis, from the minimum CoM position during leg compression within each cycle. The ground clearance indicates the maximum distance between foot and ground during flight phases. It is an indirect indicator for how dynamically the leg moves during a cycle. It can be read off of the z-coordinates of the corresponding foot contact points obtained by the simulations.

Additionally it is interesting to analyze how the peak GRF and the GRF patterns change depending on the dropping height during each bounce.

Finally, it is important to determine the peak torques arriving at the gearboxes ($\tau_{\mathrm{e,M\,Ank}}$, $\tau_{\mathrm{e,M\,Kne}}$, $\tau_{\mathrm{e,M\,Hip}}$) and the joints ($\tau_{\mathrm{e,Hip}}$, $\tau_{\mathrm{e,Kne}}$, $\tau_{\mathrm{e,Ank}}$). In the case of the stiff robot the latter variables are automatically eliminated. The joint torques are given with respect to the joint, i.e. including the combined transmission ratio, while the torques acting on the motors are given with respect to the gearbox output, i.e. including only the motor gear ratio.

These criteria and associated analyses shall mainly serve as benchmark for evaluating the passive rebound capabilities and highlighting the differences among the three models.

C. Comments regarding the Comparability of the Results

For such study it is important to ensure a valid comparability of the results among the different models. In this context, strictly speaking, the actuation of the stiff robot needs to include Coulomb friction as well [12]. But, as it is extremely difficult to determine an appropriate model for the Coulomb friction and as the target motions are rather fast, it is omitted here.

TABLE I

CONTACT MODEL PARAMETERS USED FOR THE SIMULATIONS

Vertical collision force constant	$k_{\mathrm{c}} = 8 \cdot 10^3\ \mathrm{N/m}$
Collision damping coefficient	$\lambda_{\mathrm{c}} = 10^4\ \mathrm{Ns/m^2}$
Sliding friction coefficient	$\mu_{\mathrm{fk}} = 0.6$
Sliding friction to stiction transition velocity limit	$v_{\mathrm{stic}} = 0.001\ \mathrm{m/s}$
Maximum stiction force coefficient	$\mu_{\mathrm{fs}} = 0.8$
Horizontal ground interaction stiffness	$k_{\mathrm{fs}} = 10^4\ \mathrm{N/m}$
Stiction damper	$d_{\mathrm{fs}} = 40\ \mathrm{Ns/m}$

Another important role is assigned to the controller gains. Since the controller is defined in joint space, the controller parameters are identical in all models. The conversion to motor space occurs in the controller model considering the transmission ratio z, which consists of the gear ratio and, if existent, an elastic transmission ratio. A controller for motor position θ with gain k_{p} and controller output torque τ_{c} on motor level

$$\tau_{\mathrm{c}} = (\theta_{\mathrm{d}} - \theta)\,k_{\mathrm{p}} \tag{2}$$

can be reformulated with respect to the joint side

$$\tau_{\mathrm{c,J}} = z\ \tau_{\mathrm{c,M}} = z\,(z\,{}^{\mathrm{j}}\theta_{\mathrm{d}} - z\,{}^{j}\theta)\,k_{\mathrm{p}} = ({}^{\mathrm{j}}\theta_{\mathrm{d}} - {}^{j}\theta)\,z^2 k_{\mathrm{p}} \tag{3}$$

which yields that the controller parameters are reflected to the joint side, similar to the inertia and friction, with z^2.

Note that rather stiff P and D gains were chosen for the motors. With low gains the motors are not able to keep constantly their predefined positions after ground contact, particularly when large impact forces are induced.

III. SIMULATION RESULTS

A. BioBiped1 Robot Model with Stiff Actuation

The results of the passive rebound and landing behavior of the completely stiff robot are given in Table II. Assuming a maximum possible peak torque of 12 Nm, a dropping height of only 5 cm seems to be already causing some damage to the motors. The maximum torques arriving at the gearbox of the ankle motor amounts to 13.99 Nm, significantly higher than that for the knee or hip motor. The peak torques on the gears caused by peak GRF at ground contact seem to decrease drastically for the distal joints resp. motors. Interestingly, at all different dropping heights the same hopping height[1], duty factor and flight phase duration are achieved. Note, however, that the achieved hopping heights correlate with different ground clearances, albeit not differing too widely. This is due to the increased impact forces at ground contact. As can be seen in Fig. 5, due to the larger falling heights the first contact points after falling are shifted, but the duration of the contact and flight phases are identical. Also, the

[1]These are numerically rounded values. The exact hopping heights slightly differ from the fifth decimal place onwards.

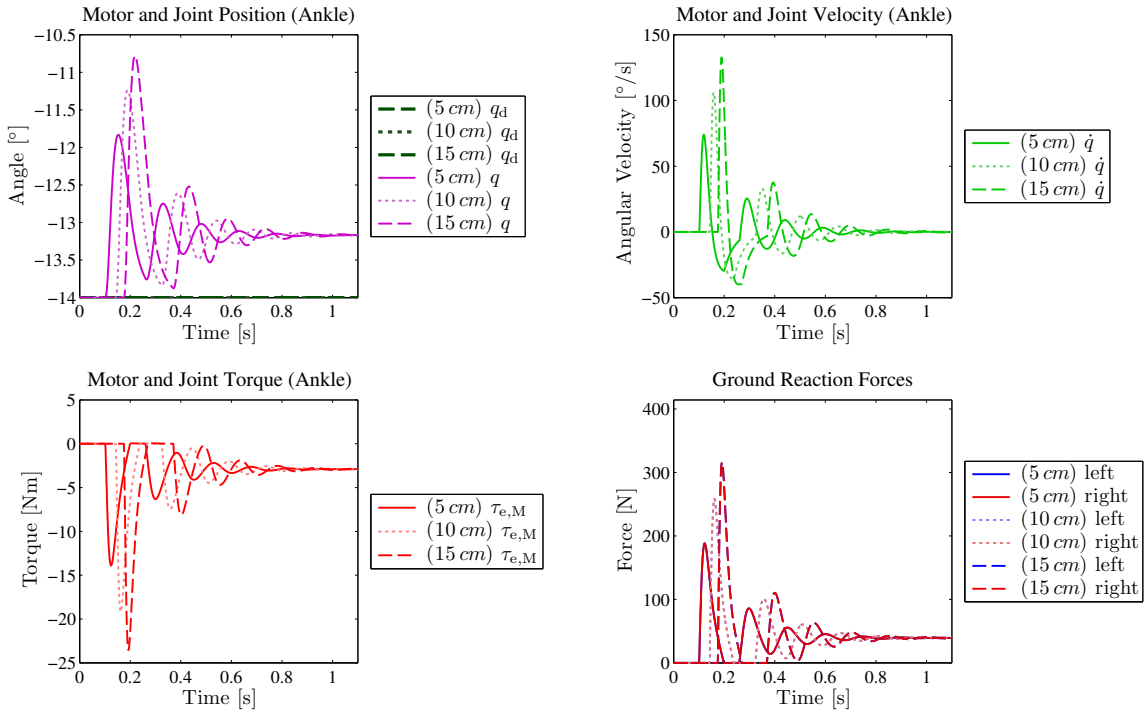

Fig. 5. Simulation results for passive rebound with the stiff robot dropped from different heights for the ankle joint. The variables q_d and q denote the desired resp. actual joint angle. $\tau_{e,M}$ stands for the generated motor torque.

TABLE II

SIMULATION RESULTS FOR PASSIVE REBOUND WITH THE STIFF ROBOT DROPPED FROM DIFFERENT HEIGHTS.

Dropping Height [m]	**Energy Restitution** [%]	**Hopping Height** [m]	**Ground Clearance** [m]	**Duty Factor** [%]	**Flight Phase** [ms]	$\tau_{e,M\,Ank}$ $\tau_{e,M\,Kne}$ $\tau_{e,M\,Hip}$ [Nm]	**GRF** [N]
0.05	17.15	0.036	0.004	52.49	85	13.89 3.67 0.95	188.32
0.10	13.12	0.036	0.009	52.49	85	19.16 4.9 1.38	258.4
0.15	11.05	0.036	0.012	52.49	85	23.54 5.91 1.73	316

energy restitution decreases for larger falling heights, i.e. more energy is dissipated. Finally, based on the peak torques given in the table it can be concluded that dropping a such stiff robot from heights larger than 5 cm can cause critical damage to the ankle motor. Besides the fact, that it can not store any energy. Note also that regardless of the falling height only one bounce is initiated by the first impact which explains the small energy restitution ratios.

B. BioBiped1 Robot Model with Rotational Series Elastic Joint Actuation

This study was repeated with the b-SEA robot with identical torsional stiffness of 87 $^{Nm}/_{rad}$ in each joint. This joint stiffness value was chosen since it corresponds to the fixed stiffness of the hip actuator transmission of the real BioBiped1 system. In contrast to the stiff robot, here the falling heights can be up to 25 cm before the torques acting on the motor gearboxes enter the range of critical values potentially damaging the motors. The falling heights can be however also even larger for less stiffer joints.

As for the GRF peaks, it can be noted that they increase less quickly than for the stiff robot. At 5 cm they are already significantly smaller and increase slower than for the stiff robot at larger falling heights. It can be also recognized that the torques at the joints agree very well with the torques on the motor of the stiff robot at this falling height proving the same simulation conditions and setup for each study. This is also true for the other falling heights the stiff robot was tested at.

Note that the energy restitution ratio increases with joint compliance, it decreases with increased falling height. In Table III we multiplied the joint stiffness values to detect the direct effects of the joint compliance at the falling height of 15 cm, which falls into the range of desired falling and subsequent hopping heights for BioBiped1's movements. It can be noticed that the energy restitution ratio diminishes rapidly with higher joint stiffness, and with it also the number of bounces from two to one. Further it can be read off of the curves in Fig. 6 and of the numbers in Table III that joint stiffness values of around 20 x 87 $^{Nm}/_{rad}$ approximately yield the passive rebound behavior of the stiff robot. The values for each performance criteria are very close.

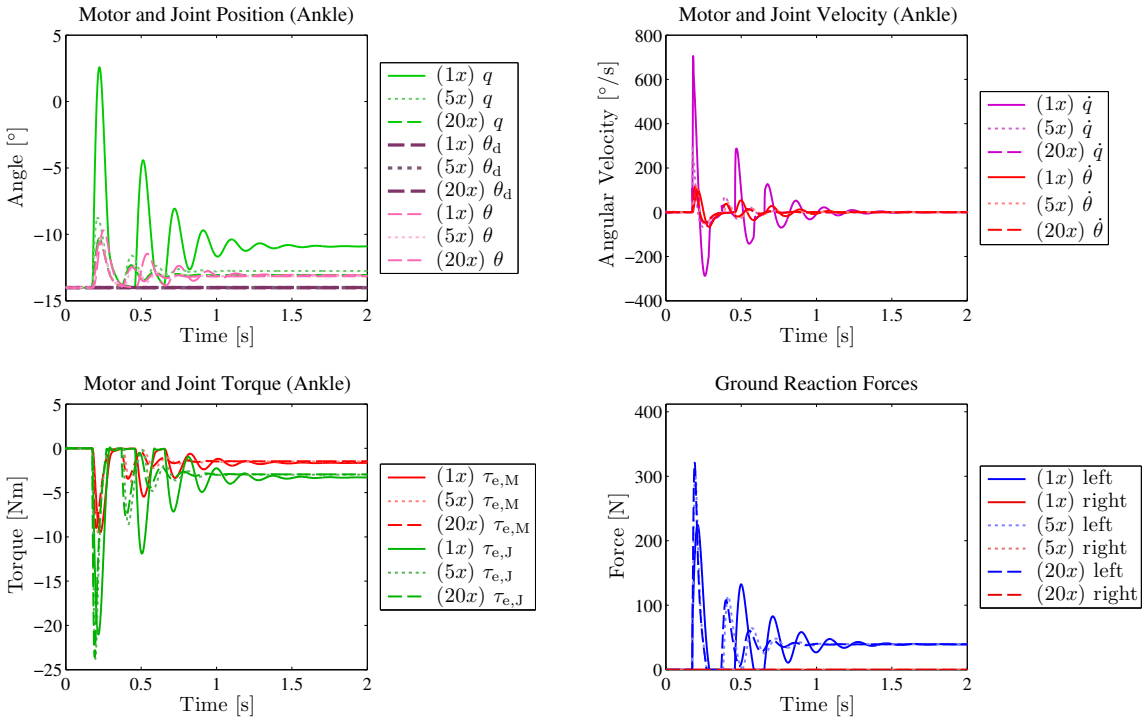

Fig. 6. Simulation results for passive rebound with the b-SEA robot with varied joint stiffnesses dropped from 15 cm for the ankle joint. $\tau_{\mathrm{e,M}}$ and $\tau_{\mathrm{e,J}}$ stand for the elastic torque exerted on the motor and the joint, respectively. θ and $\dot{\theta}$ denote the actual motor position and velocity, and θ_{d} and $\dot{\theta}_{\mathrm{d}}$ denote the desired motor position and velocity. q_{d} and q stand for the desired resp. actual joint angle.

TABLE III

SIMULATION RESULTS FOR PASSIVE REBOUND WITH THE B-SEA ROBOT WITH VARIED JOINT STIFFNESSES DROPPED FROM 15 cm.

Dropping Height [m]	$k_{\mathrm{e,Ank}}$ $k_{\mathrm{e,Kne}}$ $k_{\mathrm{e,Hip}}$ [Nm/rad]	**Bounce**	**Energy Restitution** [%]	**Hopping Height** [m]	**Ground Clearance** [m]	**Duty Factor** [%]	**Flight Phase** [ms]	$\tau_{\mathrm{e,M\,Ank}}$ $\tau_{\mathrm{e,M\,Kne}}$ $\tau_{\mathrm{e,M\,Hip}}$ ($\tau_{\mathrm{e,Ank}}$ $\tau_{\mathrm{e,Kne}}$ $\tau_{\mathrm{e,Hip}}$) [Nm]	**GRF** [N]
0.15	1 x (87 87 87)	1st	26.9	0.082	0.035	40.14	169	9.51 2.63 0.83 (21.03 6.39 1.98)	224.6
		2nd	31.99	0.034	0.006	64.10	69		132.38
0.15	5 x (87 87 87)	1st	12.71	0.048	0.014	47.09	108	9.55 2.52 0.42 (23.79 7.17 1.38)	307.78
0.15	10 x (87 87 87)	1st	11.33	0.044	0.012	48.48	101	9.22 2.4 0.39 (23.75 6.23 1.31)	317.71
0.15	20 x (87 87 87)	1st	10.71	0.043	0.011	49.48	97	8.97 2.45 0.53 (23.57 6.23 1.46)	321.11

C. BioBiped1 Robot Model with Nonlinear Elastic Tendon Actuation

With the previous study we could already demonstrate the intrinsic advantages of elastic actuation. Finally it is important to clarify how the nonlinear actuation of the knee and ankle joints in BioBiped1 together with the implemented coupled tendon elasticities can improve the above behavior. Therefore we carried out the same previous simulation runs with the BioBiped1 robot model. The exact actuation setup consists of the b-SEA in the hip (with 87 Nm/rad), the monoarticular pair of VAS (7.9 N/mm, attachment point number 5, $q_0 = -85°$) and PL (4.1 N/mm, $q_0 = -85°$) in the knee and the monoarticular pair of SOL (6.7 N/mm, attachment point number 3, $q_0 = 10°$) and TA (4.1 N/mm, $q_0 = 10°$) in the ankle. Linearization of the actuation torque vector with respect to the joint side $\boldsymbol{\tau}_{\mathrm{e,J}}$ assuming fixed motor positions $\boldsymbol{\theta} = \bar{\boldsymbol{\theta}}$ yields

$$\boldsymbol{\tau}_{\mathrm{e,J}}(\boldsymbol{q}, \dot{\boldsymbol{q}}, \boldsymbol{\theta}, \dot{\boldsymbol{\theta}}) \approx \boldsymbol{\tau}_{\mathrm{e,J}}(\bar{\boldsymbol{q}}, \bar{\boldsymbol{\theta}}) + \boldsymbol{J}_{\tau_{\mathrm{e,J}}}(\bar{\boldsymbol{q}})\,(\boldsymbol{q} - \bar{\boldsymbol{q}}) \quad (4)$$

with the actuator torque Jacobian

$$\boldsymbol{J}_{\tau_{\mathrm{e,J}}}(\bar{\boldsymbol{q}}) = \frac{\partial\, \boldsymbol{\tau}_{\mathrm{e,J}}(\boldsymbol{q}, \boldsymbol{0}, \bar{\boldsymbol{\theta}}, \boldsymbol{0})}{\partial \boldsymbol{q}}(\bar{\boldsymbol{q}}) \quad (5)$$

containing the linearized actuator output stiffnesses on joint level. For the fixed configuration of motor $\bar{\boldsymbol{\theta}}$ and joint positions $\bar{\boldsymbol{q}}$ the chosen actuation setup results in joint stiffness values of 36 Nm/rad for the knee and 19 Nm/rad for the ankle joint. This conversion allows us to compare the results with those of the b-SEA robot and shows how much softer a

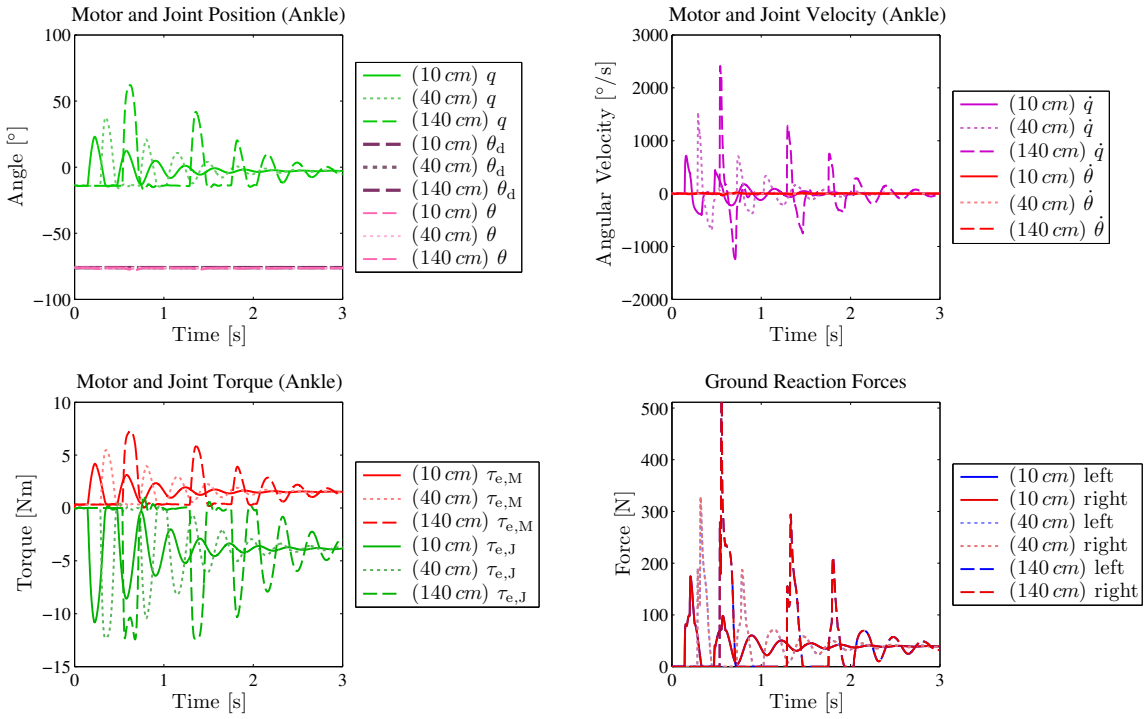

Fig. 7. Simulation results for passive rebound with the BioBiped1 robot dropped from 10 cm, 40 cm and 140 cm for the ankle joint.

typical actuation configuration of the BioBiped1 robot versus the previously simulated b-SEA robot is.

In Fig. 7 we have depicted the results for dropping heights of 10 cm, 40 cm and 140 cm for the ankle joint. The falling heights can go up to at least 1.4 m without running the risk of exceeding the maximum possible motor torque values, assuming that the segments and the overall mechanics are robust enough for the impact forces occurring at these heights which amount to approximately 13 times the body weight of BioBiped1. Further, increasing the falling heights leads only very slowly to increased torques at the gearboxes. The values start already at a much lower level for the BioBiped1 robot compared to the b-SEA robot which is due to the softer knee and ankle stiffness values. It should be also noted that the torques on the joints, $\tau_{\mathrm{e,Hip}}$, $\tau_{\mathrm{e,Kne}}$, $\tau_{\mathrm{e,Ank}}$, become extremely large while the torques on the motors remain relatively small. Especially they do not increase by the same ratio as the joint torques which is due to the highly nonlinear actuation. For instance, at the falling height of 1 m the torques on the knee joint are almost three times higher than on the coupled motor.

Note also that the energy restitution change seems to run counter to the value changes of $\tau_{\mathrm{e,M\,Ank}}$, $\tau_{\mathrm{e,M\,Kne}}$, and $\tau_{\mathrm{e,M\,Hip}}$. As the energy restitution decreases, the number of bounces increases from one to two and the torques at the gearbox continuously increase. Interestingly the increase of bounces can be detected both for the b-SEA and BioBiped1 robot at almost the same ratio of 28 % despite the different joint stiffness values.

Now let us also analyze the results obtained for stiffer knee and ankle joint configurations as depicted in Table IV. Here we chose stiffer springs for all knee and ankle tendons: VAS (15.5 N/mm, attachment point number 4, $q_0 = -75°$) and PL (8 N/mm, $q_0 = -75°$) in the knee and the monoarticular pair of SOL (15.5 N/mm, attachment point number 4, $q_0 = 20°$) and TA (6.7 N/mm, $q_0 = 20°$) in the ankle. At first sight it might be not quite understandable why the energy restitution ratio rises for increased joint stiffness in knee and ankle joints. Also the number of bounces increases up to four. In fact, the whole passive movement seem to become more dynamic, with larger hopping heights and ground clearances. Only the increase in peak torques on the motors indicates the increased joint stiffness. By analyzing the curves plotted in Fig. 8 we recognize that due to the soft ankle joint and the nonlinear actuation dynamics the GRF slightly decrease before going up to a second even higher peak. So there seems to be a trade-off between the joint stiffness values and consequently the occurring joint and motor torques and desired dynamic behavior. This example tells us that a too soft actuation, particularly of the first joint interacting with the ground, can be negative on the course of energy restitution and all the other dynamic parameters. Also too soft stiffness values cause problems for the position control in the swing phase and even stance phase. As can be seen in the curves of Fig. 8 the original positions are held much better by the stiffer configured robot (Set 2). These results allow conclusions on the optimal stiffness values to be used for actuated hopping motions. Instead of using the experimentally tuned and scaled stiffness values based on human data [8], a more sophisticated approach in order to realize an optimal dynamic locomotion behavior is to determine the optimal joint stiffness values by means of such studies.

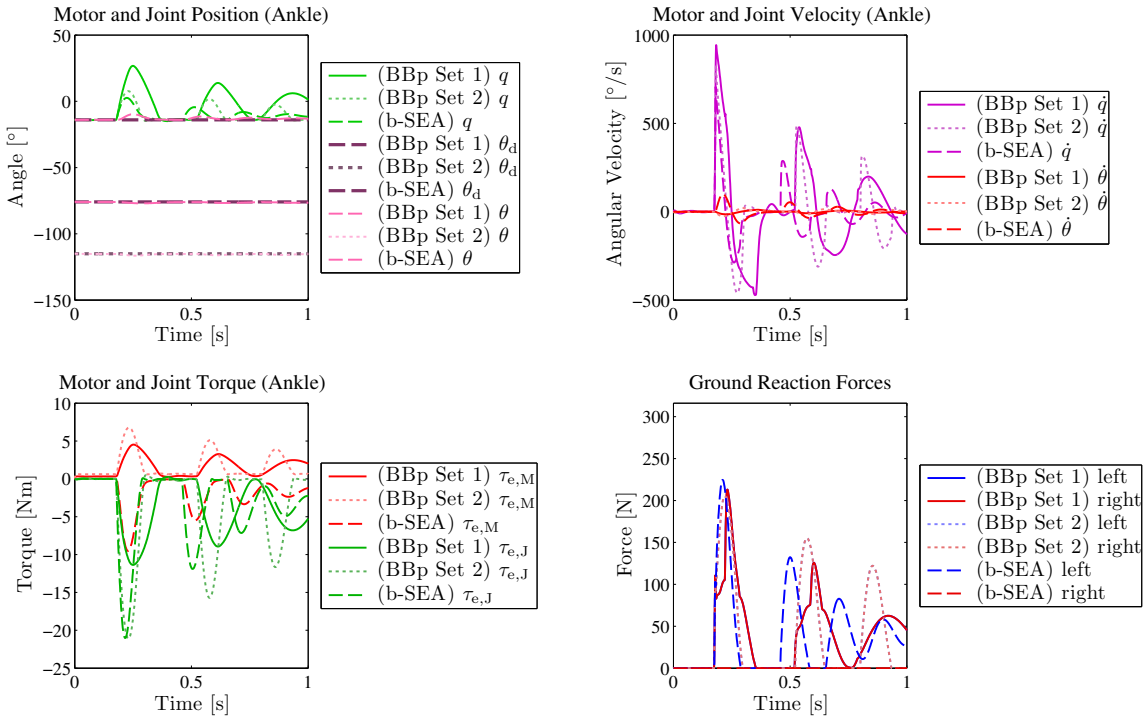

Fig. 8. Simulation results for passive rebound with the BioBiped1 robot with varied joint stiffnesses dropped from 15 cm for the ankle joint. "BBp Set 1" corresponds to the soft compliance set of 87 Nm/rad, 36 Nm/rad, 19 Nm/rad for the hip, knee and ankle joint. "BBp Set 2" corresponds to the stiffer leg actuation with 87 Nm/rad, 56 Nm/rad, 56 Nm/rad for the hip, knee and ankle joint (see also Table IV). The b-SEA robot is characterized by stiffness values of 87 Nm/rad in each joint (cf. Table III).

TABLE IV

SIMULATION RESULTS FOR PASSIVE REBOUND WITH THE BIOBIPED1 ROBOT WITH VARIED JOINT STIFFNESSES DROPPED FROM 15 cm.

Dropping Height [m]	$k_{e,Ank}$ $k_{e,Kne}$ $k_{e,Hip}$ [Nm/rad]	**Bounce**	**Energy Restitution** [%]	**Hopping Height** [m]	**Ground Clearance** [m]	**Duty Factor** [%]	**Flight Phase** [ms]	$\tau_{e,M\,Ank}$ $\tau_{e,M\,Kne}$ $\tau_{e,M\,Hip}$ ($\tau_{e,Ank}$ $\tau_{e,Kne}$ $\tau_{e,Hip}$) [Nm]	**GRF** [N]
0.15	87 36 19	1st	31.3	0.11	0.032	51.88	165	4.52 3.85 1.95 (11.36 7.16 4.46)	213.11
0.15	87 56 56	1st	44.61	0.118	0.066	35.73	222	6.77 5.63 1.57 (21.09 6.11 3.62)	205.18
		2nd	53.08	0.070	0.030	45.52	151		155.16
		3rd	54.90	0.043	0.012	57.83	96		122.13
		4th	59.08	0.028	0.003	75.25	48		96.70

IV. DISCUSSION

Summarizing this vast amount of results and drawing the most important conclusions, there is a clear interdependency between the chosen joint actuation type and the resulting dynamics behavior of the leg. Inspired by the experiment with the real robot platform, we analyzed the effects of stiff, linear elastic joint and nonlinear elastic tendon actuation for passive rebound. There was no doubt that the stiff actuation is very disadvantageous in terms of explosive energy-efficient dynamic behavior. Significant differences in the behavior could be detected between the stiff and b-SEA robot at the same falling heights. Due to the stiff actuation the impact forces are directly transmitted to the motors. Critical damage of the motors can be already expected at falling heights of 5 cm. Further, no energy can be stored from the impact.

While the energy restitution ratio increases for compliant systems, compared to stiff systems, it should be noted that it also depends on the type of actuation. For BioBiped1's nonlinear actuation dynamics a too high joint compliance can cause also high energy loss due to a chain of reactions from the GRF to the actuators absorbing too much energy whereas a linear actuation type releases the stored energy right away. Therefore spring selection also depends on the actuation type. For the specific passive rebound tests studying the landing behavior of the robot, almost identical results can be obtained for both elastic linear joint or nonlinear tendon actuation: Simulating a b-SEA robot with the parameters of "Set 2" (87 Nm/rad, 56 Nm/rad, 56 Nm/rad for the hip, knee and ankle joint) yields almost the same results as for the BioBiped1 actuation. The linearized joint stiffness values are only valid for the initial leg configuration, at ground contact

this configuration certainly changes nonlinearly according to BioBiped1's actuation dynamics, which explains the deviations from the b-SEA robot.

Yet, BioBiped1's specific actuation design is advantageous in many respects. To fully exploit the advantages of its actuation system, it is important to concentrate on a few human-like muscle-tendon functionalities. Depending on the gait not all tendons need to be implemented, as the use of all tendons may introduce timing issues that can be hardly handled. In total, the amount of passive redundant actuation should be kept at a minimum. It should be explored how actuated biarticular tendons can further reduce the complexity of the leg actuation design and improve the energy consumption while preserving the desired dynamic locomotion behavior. It is also thinkable to omit the knee motor and the passive monoarticular antagonist and instead to implement passive biarticular tendons spanning the knee joint.

It is important to note that for best results for a specific motion realization it may be necessary due to the vast amount of "regulating screws" to apply a kind of "cascaded optimization", e.g. first the actuation is optimized with respect to criteria such as energy restitution, hopping height, and ground clearance and subsequently the controller gains are optimized for low amount of actuators' efforts keeping the torques on the motors as low as possible. On the other hand, the decrease in torques comes at the cost of less precise position control, which is important particularly during swing phase. Also, too low controller gains lead to shocks being almost completely absorbed, e.g. further bounces would be hardly detectable.

Another important advantage of compliant actuation is that provided energy recovery mechanisms the amount of energy storage can be further increased.

In literature we could not find any similar studies except of Niiyama's work in [5]. The pneumatically driven robot was dropped from one meter. It was argued that soft landing was possible, accompanied by snapshots of the falling and landing, because of exploitation of the anti-gravity muscles and compliance. The study did not include any diagrams or tables with more in-depth information about the experimental setup and forces and torques involved.

Varying the compliance of an actuator by software control of a stiff actuator is currently a less favorable option, as this type of compliant actuator requires the actuators, sensors and controllers to be all fast enough for the application. In our studies the falling times vary between 102 ms and 227 ms depending on the falling height. The various components of a complex bipedal system need to react within these time delays. Additionally, it should be kept in mind that even if the bandwidth of the actively controlled compliance was not limited to the bandwidth of the sensors, actuators and controllers, it dissipates energy and cannot reduce impacts. Thus, passive compliance is considered as essential requirement for intrinsic compliance. However, it should be also mentioned that several research groups have successfully applied active compliance for high-speed locomotion [13], [14].

V. Conclusions

In this paper we investigated the beneficial properties of compliant actuation for dynamically locomoting bipedal robots. Shock tolerance and energy storage and release belong to the most important capabilities of a dynamically moving, but also energy-efficient robot. In extensive simulation studies we highlighted the many advantages of elastic over stiff actuation for soft landing and passive rebound. Further the differences between linear elastic joint and nonlinear elastic tendon actuation were discussed. As a guideline for choosing an optimal leg actuation design and parameter setting, passive rebound tests can be carried out to analyze and modify the locomotor function as desired. Future work comprises the use of optimization and learning techniques to further improve the actuation parameters to yield the most dynamic and energy-efficient locomotion performance.

Acknowledgments

This work has been supported by the German Research Foundation (DFG) under grant no. STR 533/7-1. The authors thank Thomas Lens for the helpful discussions.

References

[1] G. A. Pratt and M. M. Williamson, "Series elastic actuators," in *IEEE International Workshop on Intelligent Robots and Systems*, 1995, pp. 399–406.

[2] M. H. Raibert, *Legged robots that balance*. MIT Press, 1986.

[3] C.-M. Chew, J. Pratt, and G. Pratt, "Blind walking of a planar bipedal robot on sloped terrain," in *Proc. IEEE Int. Conf. Robotics and Automation*, 1999, pp. 381 – 386.

[4] J. W. Hurst and A. A. Rizzi, "Series compliance for an efficient running gait," *IEEE Robot. Autom. Mag.*, vol. 15, no. 3, pp. 42–51, 2008.

[5] R. Niiyama, "Design of a musculoskeletal Athlete robot: A biomechanical approach," in *Int. Conf. Climbing and Walking Robots and the Support Technologies for Mobile Machines*, 2009, pp. 173–180.

[6] K. Hosoda, Y. Sakaguchi, H. Takayama, and T. Takumai, "Pneumatic-driven jumping robot with anthropomorphic muscular skeleton structure," *Autonomous Robots*, vol. 28, no. 3, pp. 307–316, 2010.

[7] M. Hutter, C. Remy, M. Hoepflinger, and R. Siegwart, "High compliant series elastic actuation for the robotic leg ScarlETH," in *Int. Conf. Climbing and Walking Robots and the Support Technologies for Mobile Machines*, 2011.

[8] K. Radkhah, C. Maufroy, M. Maus, D. Scholz, A. Seyfarth, and O. von Stryk, "Concept and design of the BioBiped1 robot for human-like walking and running," *International Journal of Humanoid Robotics*, vol. 8, no. 3, pp. 439–458, 2011. [Online]. Available: http://www.worldscinet.com/ijhr/08/0803/S0219843611002587.html

[9] Biobiped project website. [Online]. Available: www.biobiped.de

[10] K. Radkhah, T. Lens, and O. von Stryk, "Detailed dynamics modeling of BioBiped's monoarticular and biarticular tendon-driven actuation system," in *Proc. IEEE/RSJ Int. Conf. Intelligent Robots and Systems*, October 7 - 12 2012, pp. 4243 – 4250.

[11] T. Lens, K. Radkhah, and O. von Stryk, "Simulation of dynamics and realistic contact forces for manipulators and legged robots with high joint elasticity," in *International Conference on Advanced Robotics (ICAR)*, June 20-23 2011, pp. 34–41.

[12] A. Albu-Schäffer, "Regelung von Robotern mit elastischen Gelenken am Beispiel der DLR-Leichtbauarme," Ph.D. dissertation, Technische Universität München, 2002.

[13] S. Seok, A. Wang, D. Otten, and S. Kim, "Actuator design for high force proprioceptive control in fast legged locomotion," in *Proc. IEEE/RSJ Int. Conf. Intelligent Robots and Systems*, 2012, pp. 1970–1975.

[14] "BigDog - The most advanced rough-terrain robot on earth," http://www.bostondynamics.com/robot_bigdog.html.